coatings

MDPI

Article

Intense Laser Field Effect on the Photo-Ionization Cross-Section of the First Exciton Transition in a Core/Shell Quantum Dot Submitted to an Applied Electric Field

Laura M. Pérez [1,*], Noreddine Aghoutane[2,*], David Laroze [2], Pablo Díaz [3] and Mohamed El-Yadri [4] and EL Mustapha Feddi [4,5]

1 Departamento de Física, FACI, Universidad de Tarapacá, Casilla 7D, Arica 1000000, Chile
2 Instituto de Alta Investigación, Universidad de Tarapacá, Casilla 7D, Arica 1000000, Chile; dlarozen@uta.cl
3 Departamento de Ciencias Físicas, Universidad de La Frontera, Casilla 54-D, Temuco 4780000, Chile; pablo.diaz@ufrontera.cl
4 Group of Optoelectronic of Semiconductors and Nanomaterials, ENSAM, Mohammed V University, Rabat 10100, Morocco; m.elyadri@um5r.ac.ma (M.E.-Y.); e.feddi@um5r.ac.ma (E.M.F.)
5 Institute of Applied Physics, Mohammed VI Polytechnic University, Ben Guerir 43150, Morocco
* Correspondence: lperez@uta.cl (L.M.P.); noreddine.aghoutane@gmail.com (N.A.)

Abstract: In the current work, we study the intense laser pulse influences on the behaviors of the first excitonic transition in a core/shell quantum dot submitted to an electric field. Therefore, the exciton binding energy and the mean distance between the correlated electron–hole pair are discussed, considering the electric field and laser strength. Our calculations show that both external fields play significant repulsive effects. Through their effects, they oppose the attractive nature of the Coulomb potential between the correlated pair, which decreases the excitonic binding energy. We also analyze the dissociation process by determining the photo-ionization cross-section (PICS). Our findings show that the peaks of the PICS redshift when the shell thickness $b - a$ increases. For a given core radius, the laser and electric field induce a shift toward the low-energy region for the PICS; this displacement is more pronounced for the laser case. Our study also compares simple quantum dots and core/shell quantum dots to show the effect of the inner radius on the obtained results. Our theoretical results can lead to promising applications of exciton-based devices controlled by sizes and external fields.

Keywords: core/shell quantum dots; exciton; Intense laser field; electric field; photo-ionization cross-section; exciton binding energy

Citation: Pérez, L.M.; Aghoutane, N.; Laroze, D.; Díaz, P.; El-Yadri, M.; Feddi, E.M. Intense Laser Field Effect on the Photo-Ionization Cross-Section of the First Exciton Transition in a Core/Shell Quantum Dot Submitted to an Applied Electric Field. *Coatings* **2023**, *13*, 1098. https://doi.org/10.3390/coatings13061098

Academic Editors: Supab Choopun, Sukrit Sucharitakul and Emerson Coy

Received: 28 April 2023
Revised: 11 June 2023
Accepted: 12 June 2023
Published: 14 June 2023

1. Introduction

Low-dimensional systems have attracted great interest in materials science after being studied extensively, either theoretically or experimentally [1–8]. These systems are classified according to the degree of confinement of particles as 1D (quantum wells (QW)), 2D (quantum wires), and 3D (quantum dots (QD)). The increasing interest in these structures, especially QD, is due to their wide technological applications, such as memory devices, solar cells, and terahertz detectors [9,10]. Nevertheless, the modest chemical/photostability of QDs in the presence of air and moisture hinders their use and exploitation. Therefore, to increase the stability of these QDs, several approaches have been developed during the last few decades. These approaches allow for achieving new architectural configurations by coating a second material onto QDs, known as core/shell quantum dots (CSQD), which have been demonstrated to be an effective method for enhancing QD photostability and improving absorption at various wavelengths and with more accurate colors [11–16]. Therefore, due to their intriguing morphological features, which can be controlled based on shapes and thickness, this nanostructure has garnered interest because of the combination of several exceptional qualities that individual components do not possess. These systems may integrate the traits and qualities of both the coated shell and the core, where the shell

surface properties can be translated to the core or vice versa, giving these structures new performances and functionalities. Depending on these properties, these classes of materials have been utilized in numerous applications such as surface coatings, light-emitting diodes, printing, corrosion protection, impact modifiers, and sensing, to mention a few [17–20]. The excitation of QDs can create an electron–hole correlated pair (exciton). From their extensive intervention in the optical process, the excitons offer a better comprehension of physical properties, such as excitonic binding energy (E_b) and photo-ionization cross-section (PICS), which is considered an important factor in the understanding of optoelectronic properties of these types of CSQD structures [21–26].

In addition to the choice of the materials, adjusting particle size and shape is a very important factor in the synthesis or processing steps of QDs, because the physical properties of core/shell particles are much more sensitive to their size and shape. Many studies have shown that nanoparticle size can be controlled by varying the laser photon energy (wavelength), where the particle size decreases as the number of irradiations of laser pulses increases [27–30]. Moreover, the intense laser (ILF) and electric fields (EF) induce repulsive effects that counteract the attractive Coulomb interaction between the correlated pair, reducing the overall E_b, and therefore affecting the physical properties of these nanomaterials [31–39]. The influence of these two applied fields on some nanostructures has been widely investigated in the literature [40–44]. In particular, the effect of ILF was analyzed for quantum rings by Radu et al., finding an analytical expression for the dressed potential [31]. The combined effects of EFs and ILFs on cylindrical QDs were studied, in which the nonlinear optical properties were computed [32]. Barseghyan et al. explored double QD electronic and optical properties, considering a lateral EF and ILF [33]. Moreover, Laroze et al. examined the states of impurity in 2D QDs and quantum rings [40]. A theoretical study of a donor dopant inside a QD under the excitation of an ILF was carried out by Yesilgul et al. [45]. They found a strong impact of the ILF on the interaction of electron impurity, which manifests in a variation in the donor E_b. The impurities' nonlinear properties of QD using an ILF were investigated by Lu et al. [46,47]. Their findings indicate that these properties respond sensitively to the ILF. Later, Burileanu reported the effect of EF and ILF on the PICS of a donor in QDs [48]. Wang et al. studied the impact of ILF on PICS of donor dopants in semiconductors [49]. They demonstrated that the PICSs shift to the lower energy of the photon when the laser intensity augments. Xie investigated the susceptibility and PICS of an exciton in a QD; he observed that the dot size and hole mass have a strong effect on the exciton susceptibility and PICS [24]. The magnetic field (B) impact on the PICS of exciton within quantum wire was discussed by Arunachalam et al. [25]. Another study was carried out by Angayarkanni concerning the pressure-dependent PICS for an exciton in a QW; they found that well width and hydrostatic strain had a significant influence on the PICSs [26]. Isono et al. realized the photo-ionization of the singlet exciton in single-crystal naphthalene; they showed that the cross-section increases monotonically with the photon energy [50]. The EF effect on the fundamental state energy of a donor dopant within QD was examined by Feddi et al. [51]. Additionally, M'zerd et al. realized the EF effect on the PICS of a dopant in a CSQD; their results show that the PICS spectra exhibit a redshift when the EF is applied [52].

However, among the available research, most of the reports focused on impurities; only some examined the ILF effect on excitons confined in QDs. Ouadghi et al. studied the E_b of excitons in a simple QD under an ILF. They reported that the ILF lowers the excitonic E_b [53]. The ILF effects on the exciton E_b in QW were reported by Yesilgul et al.; their results show that the ILF has a significant effect on the physical properties of an exciton in the QW [54]. Concerning the EF effect on excitons, Heyn et al. studied the states of excitons in conical QDs under applied EF and B [55]. The EF effect on exciton states in CSDQs has been investigated for CdSe/ZnS and InGaAsP/InP materials [56,57]. These studies have shown a profound dependency between the excitonic properties and the applied EF.

To our best knowledge, no studies have been carried out that treat the ILF impact on the properties of an exciton confined in a spherical CSQD. For this reason, this study

is regarded as a contribution to the comprehension of the behaviors of the E_b and PICSs of excitons within these types of structures under the application of ILF and EF. Our computations have been made in the effective mass framework and the variational method and by selecting a good wave function considering the correlation of particles, the laser intensity, and the EF effect. This research paper starts with the introduction. The theoretical model of the calculations is given in Section 2. The discussions of our findings are reported in Section 3.

2. Background Theory

This research is based on an exciton trapped in a spherical CSQD formed by AlAs/GaAs/AlAs with AlAs of radius a and GaAs of radius b representing the core and shell, respectively. Our system is submitted to a uniform external EF and an ILF. The Hamiltonian of this CSQD in the existence of these two fields can be written as:

$$H_X = -\frac{\hbar^2}{2m_e^*}\Delta_e - \frac{\hbar^2}{2m_h^*}\Delta_h + V_c(\overrightarrow{\alpha}) + W_i + V_w^i \tag{1}$$

$V_c(\overrightarrow{\alpha})$ is the dressed Coulomb potential describing the interaction energy of correlated pair under the influence of the ILF of amplitude A_0 and angular frequency Ω. This dressed Coulomb interaction is given by [48,58]:

$$V_c(\overrightarrow{\alpha}) = \frac{-e^2}{\varepsilon}\left(\frac{1}{|\overrightarrow{r_e} - \overrightarrow{r_h} + \overrightarrow{\alpha}|} + \frac{1}{|\overrightarrow{r_e} - \overrightarrow{r_h} - \overrightarrow{\alpha}|}\right) \tag{2}$$

where $\overrightarrow{r_e}$ ($\overrightarrow{r_h}$) is the electron (hole) position. $\alpha = eA_0/\mu\Omega = (8\pi e^2 I/\mu^2 c\Omega^4)^{1/2}$ is assessed as a factor that establishes the ILF strength, known as the laser-dressing parameter, which has a nanometer (angström) unit. It includes both the frequency Ω and intensity of the laser I (kW/cm^2); c is the light velocity and $\mu = (\frac{1}{m_e^*} + \frac{1}{m_h^*})^{-1}$ is the exciton reduced mass.

$V_w^i = V_w^e + V_w^h$ is the potential confinement of electron and hole, respectively, and it is given as follows:

$$V_w^i = \begin{cases} 0 & a < r_i < b \\ \infty & 0 < r_i < a \text{ and } r_i > b \end{cases} \quad i = (e,h) \tag{3}$$

a (b) is the CSQD's internal (external) radius. The infinite potential choice is justified by very large-band offsets of the heterostructures, where particles always remain confined to the shell region.

W_i $(i = e,h)$ represents the dipolar electrostatic energy of the particles, given by:

$$W_i = W_e + W_h = e\overrightarrow{F} \cdot (\overrightarrow{r_e} - \overrightarrow{r_h})). \tag{4}$$

Using the excitonic units $a_X = \hbar^2\varepsilon/e^2\mu$ for length and $R_X^* = \hbar^2/2\mu a_X^2$ for energy, as well as the dimensionless parameter $f = ea_X^*/R_X^*$ (which measure of the EF in the effective units), the Hamiltonian (1) becomes:

$$\begin{aligned} H_X \quad = \quad & -\frac{1}{(1+\sigma_1)}\Delta_e - \frac{\sigma_1}{(1+\sigma_1)}\Delta_h - \\ & \left(\frac{1}{|\overrightarrow{r_e} - \overrightarrow{r_h} + \overrightarrow{\alpha}|} + \frac{1}{|\overrightarrow{r_e} - \overrightarrow{r_h} - \overrightarrow{\alpha}|}\right) + W_i + V_w^i \end{aligned} \tag{5}$$

where $\sigma_1 = m_e^*/m_h^*$ is the mass ratio and W_i follows the expression:

$$W_i = e\overrightarrow{F} \cdot (\overrightarrow{r_e} - \overrightarrow{r_h}) = f(z_e - z_h) \tag{6}$$

The coordinates Hylleraas (r_e, r_h, r_{eh}, z_e, z_h) are a very good choice for describing a two-bodies system [21–23], and therefore, the Laplacian for the electron (for the hole, the index e is substituted by h) is given by:

$$\begin{aligned}\Delta_e &= \frac{\partial^2}{\partial r_e^2} + \frac{\partial^2}{\partial r_{eh}^2} + \left(\frac{r_e^2 - r_h^2 + r_{eh}^2}{r_e r_{eh}}\right)\frac{\partial^2}{\partial r_e \partial r_{eh}} + \frac{2}{r_e}\frac{\partial}{\partial r_e} \\ &+ \frac{2}{r_{eh}}\frac{\partial}{\partial r_{eh}} + \frac{2z_e}{r_e}\frac{\partial^2}{\partial z_e \partial r_e} + 2\left(\frac{z_e - z_h}{r_{eh}}\right)\frac{\partial^2}{\partial z_e \partial r_{eh}} + \frac{\partial^2}{\partial z_e^2}\end{aligned} \tag{7}$$

The fundamental energy of exciton E_X and the corresponding wave function Ψ_X can be calculated from the equation of Schrödinger: $H_X\Psi_X = E_X\Psi_X$. Without an analytical solution, this equation must be solved numerically. The chosen numerical method in this work concerns the variational method with an appropriate wave function. The exciton's fundamental energy can be determined by the minimization of the value of H_X:

$$E_X = \min_{\beta,\eta,\lambda} \frac{\langle \Psi_X | H_X | \Psi_X \rangle}{\langle \Psi_X | \Psi_X \rangle} \tag{8}$$

To describe the distortion entered by the ILF and EF, the trial wave functions are given as:

$$\Psi_X = N_1 J_0(r_e) Y_0^0(\theta_e, \varphi_e) J_0(r_h) Y_0^0(\theta_h, \varphi_h) e^{-\beta r_{eh}} e^{\eta f(z_e - z_h)} e^{\lambda(z_e - z_h)} \tag{9}$$

J_0 and Y_0^0 are spherical Bessel of order zero and harmonic functions, respectively. N_1 is the normalization constant. $e^{-\beta r_{eh}}$ refers to the Coulomb correlations between the particles. $e^{-\eta f(z_e - z_h)}$ and $e^{\lambda(z_e - z_h)}$ depict the impact of the EF and ILF on the particles. β, η, and λ are the variational parameters, which must be determined for minimizing the energy E_X. The exciton E_b is then given by:

$$E_b = E_e + E_h - E_X \tag{10}$$

The photo-ionization cross-section (PICS) refers to the removal of a particle from its electronic state by the action of light, and it is governed by a dipole transition between the states. This PICS is a crucial process in a vast range of phenomena. It is the simplest process that gives detailed information about complexes excitonic, and it is mainly utilized in the characterization of semiconductor materials. In the dipole approximation, the PICS can be written as [59,60]:

$$\sigma(\hbar\omega) = \frac{4\pi e^2}{n_r \hbar c}\left(\frac{F_{eff}}{F_0}\right)\hbar\omega \times \sum \left| \langle \Psi_i | \overrightarrow{\zeta}.\overrightarrow{r_i} \left| \Psi_f \right\rangle \right|^2 \delta(E_f - E_i - \hbar\omega) \tag{11}$$

where $\hbar\omega$ is the photon energy of excitation, n_r is the index of refraction, and F_{eff}/F_0 is the ratio between electromagnetic radiation's effective electrical component and the mean EF. $\langle \Psi_i | \overrightarrow{\zeta}.\overrightarrow{r_i} \left| \Psi_f \right\rangle$ $(i = e, h)$ is the transition state's dipole moment's matrix component. $\overrightarrow{\zeta}$ is the light wave vector's polarization. Ψ_f is the eigenfunction of the Hamiltonian given by Equation (1) without the Coulombic interaction effect, while the initial state Ψ_i refers to the exciton wave function (expression (9)). Please note that $\langle \Psi_i | \overrightarrow{\zeta}.\overrightarrow{r_i} \left| \Psi_f \right\rangle$ depends deeply on the polarization orientation controlled by the strict selection rules. For simplicity, we accept in our study that the polarization is along the z-axis; in this case, the PICS is given as:

$$\sigma(\hbar\omega) = \frac{4\pi e^2}{n_r \hbar c}\left(\frac{F_{eff}}{F_0}\right)\hbar\omega \times I_{OP}\frac{\Gamma}{(E_b - \hbar\omega)^2 + \Gamma^2} \tag{12}$$

where Γ represents the maximum line width of the Lorentzian at midheight. I_{OP} is the optical integral of the recombination of the pair, given by the following expression:

$$I_{OP} = \left| \int_V \Psi_i(r_e, r_h)(z_e + z_h)\Psi_f(r_e, r_h, r_{eh}) dr_e dr_h dr_{eh} \right|^2 \quad (13)$$

The PICS determination first requires calculating the effective field parameter F_{eff} at the exciton site, which is very heterogeneous and tricky to calculate because the external field related to the incoming radiation has three spatial components along all polarization orientations. There is little knowledge about how the laser influences the F_{eff}/F_0 ratio in such laser-driven materials. Since the form of the PICS is not influenced by the F_{eff}, we consider $F_{eff}/F_0 = 1$.

3. Discussion of Results

This work aims to highlight the impact of an ILF on an exciton confined within a spherical CSQD submitted to a uniform EF, where the physical parameters of the studied GaAs material are given in Table 1 [61].

Table 1. Physical parameters of the studied material.

E_g (eV)	m_e^*/m_0	m_h^*/m_0	ε	R_X (meV)	a_X (nm)
1.607	0.067	0.079	13.18	2.84	21.78

In the first approach, let us start our investigation with the case of the simple GaAs QD (SQD) ($a = 0$). In Figure 1a,b, we present E_b of the exciton, for several EF and ILF values, respectively. As a first remark, the excitonic E_b enhances as the size of QD (b) decreases. This evolution is related to the effect of the confinement, where for the smallest dots, the exciton wave function becomes strongly localized within it, and the three-dimensional (bulk) values limits (=1R_X) are reached for large QD sizes. By examining the ILF effect, we notice that E_b is a decreasing function with the α parameter because of the system's geometric modifications brought on by the laser, which influences the exciton wave function's localization within the QD. As a result, the Coulombic interaction between the particles becomes weak, i.e., the charge carriers are less confined under the application of ILF. Moreover, we note that the laser effect is always pronounced, even for strong confinement regions. (Our findings are consistent with those obtained for the impurity [62,63]). Regarding the EF effect (Figure 1b), we find that for a strong confinement regime ($b < 1.5a_X$), E_b decreases quickly, and the confinement effect is more critical than the EF one (EF effect seems to be negligible). However, when the QD size increases, the confinement loses dominance, and the EF effect is further evident because of the expansion of the excitonic orbital close to the surface of the QD, and thus E_b is more sensitive to EF in this case. The external EF and ILF can modify the quantum states of particles trapped in very low-dimensional materials. Moreover, they are powerful tools for investigating the properties of the complexes excitonic confined in CSQD. It is well known that the electronic system confinement potential is significantly altered when an ILF is used to irradiate it. This has a strong impact on the Colombian interactions between the particles, which leads to a modification in the CSQDs' physical properties.

Next, the laser effect on the core/shell QD configuration is discussed. In Figure 2a, we show the variation of the exciton's E_b in relation to the ratio a/b, for $b = 2a_X$, and for $\alpha = 0, 5$ and 10 nm. We remark that at zero applied laser field, the E_b variation includes two regions separated by a minimum corresponding to a/b_{cri}, where when a/b varies from a/b_{cri} to 1, E_b tends towards the well-known $2D$ exciton E_b limits (=4R_X), i.e., the particles form a free rotation over the surface of the well of GaAs, and consequently, the kinetic energy becomes more important than the Coulomb energy, leading to an augmentation in the exciton E_b. The rise of E_b over the a/b_{cri} indicates that the system behaves as two-dimensional ($2D$) material created by some layers of $GaAs$. This a/b_{cri} value allows us to distinguish between the $3D$ geometrical system and spherical surface confinement. According to the above assertions, the laser application shows a drastic reduction in

the excitonic E_b, especially within the $a/b > 0.4$ limits, because of the weakness of the confinement induced by the geometrical change resulting from the applying ILF. We also see that the E_b minimum shifts to the higher values of a/b as α increases. In Figure 2b, the EF effect on the exciton E_b of a CSQD is plotted for $b = 2a_X$ and different values of EF ($F = 0, 5$ and 10 kV/cm). It is observed that E_b diminishes with EF augmentation. Indeed, the application of the EF diminishes the influence of the confinement for both particles because of the increase in the structure size; therefore, E_b reduces. This decrease is more pronounced when a/b tends to 1 but is still inferior to that obtained in the ILF application case (Figure 2a).

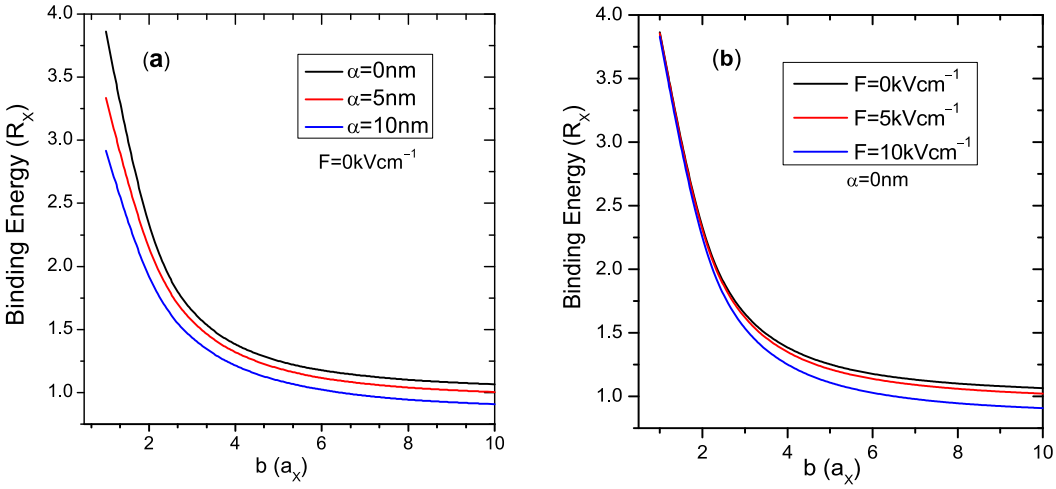

Figure 1. Excitonic E_b variation versus the QD radius b. (**a**) For $\alpha = 0, 5$ and 10 nm. (**b**) For $F = 0, 5$ and 10 kV/cm.

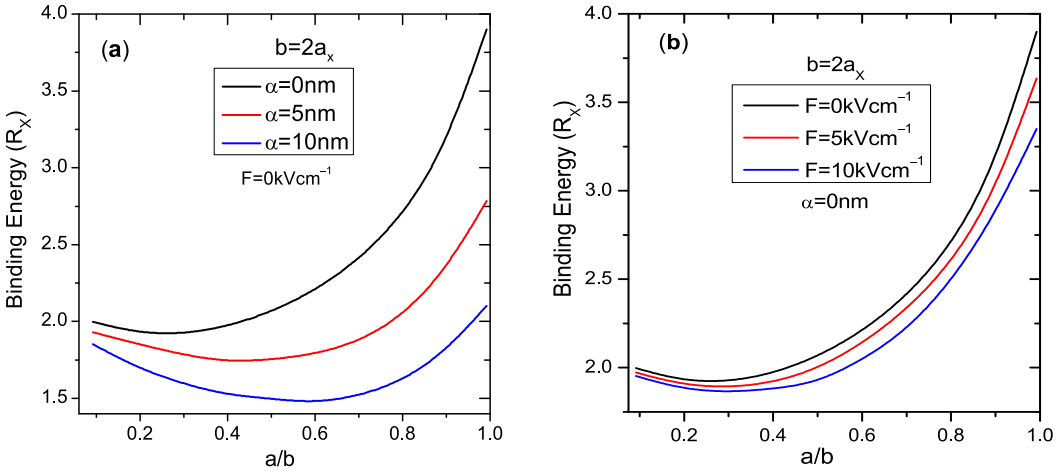

Figure 2. Excitonic E_b variation versus the core/shell radii ratio a/b for $b = 2a_X$. (**a**) For $\alpha = 0, 5$ and 10 nm. (**b**) For $F = 0, 5$ and 10 kV/cm.

The analysis of the variation of the particles' mean distances can support the excitonic E_b behaviors. In Figure 3, we plot the electron–hole mean distance $\langle r_{eh} \rangle$ given as $\langle r_{eh} \rangle = \frac{\langle \Psi_X | r_{eh} | \Psi_X \rangle}{\langle \Psi_X | \Psi_X \rangle}$, for a simple QD (a) and a core/shell QD (b). We remark that for the strong confinement region ($b < 1.5a_X$ for simple QD and $a/b \simeq 1$ for CSQD), the distance $\langle r_{eh} \rangle$ is small because the particles are unable to penetrate the well barriers due to the infinite potential confinement, and therefore, the electron and hole become very close to each other. When the ILF and EF are applied, it is noted that $\langle r_{eh} \rangle$ increases for both structures (this increase is more significant for the ILF than for the EF), i.e., with EF and ILF presence, the exciton is less confined because of the dispersion of the wave function s surrounding the QD well, leading to a decrease in the interaction between the particles. In

summary, both fields weaken the pair interaction, which explains the drop in the binding energy when these fields are applied.

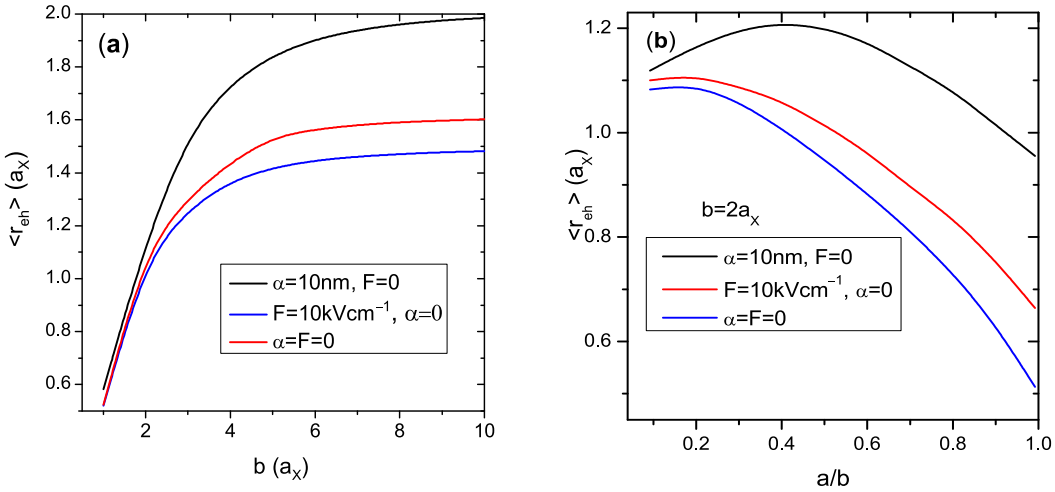

Figure 3. Variation of the average distance $\langle r_{eh} \rangle$, for $\alpha = F = 0$, $\alpha = 10$ and $F = 10$ kV/cm for simple QD (**a**) and for CSQD (**b**).

The following topic is photo-ionization cross-section (PICS) behaviors analysis. Its measurement in the nanostructures system is important for comprehending the optical properties of charge carriers within QDs. First, it should be noted that the PICS depends essentially on E_b and the optical integral (I_{OP}) variations (Equation (12)). Figure 4a shows the evolution of the PICS of the exciton in relation to the photon energy of excitation $\hbar\omega$, for an SQD (with radius b), and $b = 1, 2$ and $3a_X$, in the absence of external perturbations. One can see that the PICS peaks are deeply influenced by the SQD sizes, where the decrease in the structure volume induces a remarkable blue shift (the PICS spectrum moved towards higher energy regions). These behaviors are related to the sensitivity of exciton E_b with the QD size variations. The application of the EF and ILF to the system (Figure 4b and 4c, respectively) show clearly an important impact on the PICS, where under the influence of these two external factors, the PICS peaks show a redshift, i.e., the $\hbar\omega$ value corresponding to the peak of the PICS shifts to the region of lower energies, because, as mentioned above, the ILF and EF increase the electron–hole distance. Consequently, the Coulomb interaction of the pair is weakened, and the excitonic E_b correspondingly reduces. Therefore, a redshift of the PICS peak appears. Additionally, we see that the PICS peak intensities reduced (enhanced) with the ILF and EF application (QD radius increment) due to I_{OP} variation. For this reason, we plot in Figure 4d the I_{OP} variation for $\alpha = 0, F = 0$, $\alpha = 10$ nm and $F = 10$ kVcm^{-1}. As we can observe from this figure, I_{OP} increases with QD sizes while the ILF and EF reduce it, which leads to the changes observed in the intensity of the PICS peaks.

In Figure 5a, we examine the PICS according to the core–shell sizes, where we trace their evolutions versus $\hbar\omega$ energy for $b = 1, 2$ and $3a_X$ and $a = 0.5a_X$, without ILF and EF effects. First, note that the threshold frequency and intensity of the peak depend on both shell radius b and shell thickness $b - a$. This figure indicates that the PICS exhibits a resonant peak at the incident photon energy threshold frequency when $\hbar\omega = E_b$. In addition, as $b - a$ increases, the PICS peak shows a redshift due to the E_b and the superposition of the wave function variations under the effect of structural confinement. By comparing the two curves corresponding to $a = 0$ (simple QD) and $a = 0.5a_X$ (CSQD), we find that the peak threshold moves from $\hbar\omega \simeq 15.53$ meV to $\simeq 8.54$ meV for $b = 1a_X$, from $\hbar\omega \simeq 8.9$ meV to $\simeq 5.2$ meV for $b = 2a_X$ and from $\hbar\omega \simeq 6.3$ meV to $\simeq 4.1$ meV for $b = 3a_X$, respectively. The peak shifts between QD and CSQD are more important for the smaller radii than the larger ones. These behaviors are related to the difference in E_b and I_{OP} values between the SQD and CSQD (Figures 1 and 2). The ILF and EF effects on the PICS of an exciton confined in a CSQD are plotted in Figure 5b,c for shell thickness $b - a = 1.5a_X$. The application of

these two external perturbations significantly affects the PICS threshold values, where the peaks are shifted to the low-energy regions of the incident photons. It is known that the application of an ILF and EF on a QD provokes a change in the system geometry, which reduces the confinement and, therefore, induces a spacing between the electron and hole (augmentation of the distance $\langle r_{eh} \rangle$ (Figure 3b)), which leads to a decrease in exciton E_b. Consequently, a redshift of the PICS peaks is remarked when the ILF and EF are applied. In Figure 5d, the I_{OP} variations are presented in relation to the ratio a/b. We find that the applied ILF and EF reduce the optical integral, particularly for the small values of a/b. This I_{OP} behavior explains the reduction in PICS peak intensities under ILF and EF effects, obtained in Figure 5b,c. Finally, we should note that the peak resonance positions are within the $3.76 - 0.99$ terahertz range, corresponding to the low THz frequencies. These outcomes give another level of opportunity for different device applications of low THz frequencies, such as terahertz detectors, by adjusting the applied external fields and sizes of the CSQD structure.

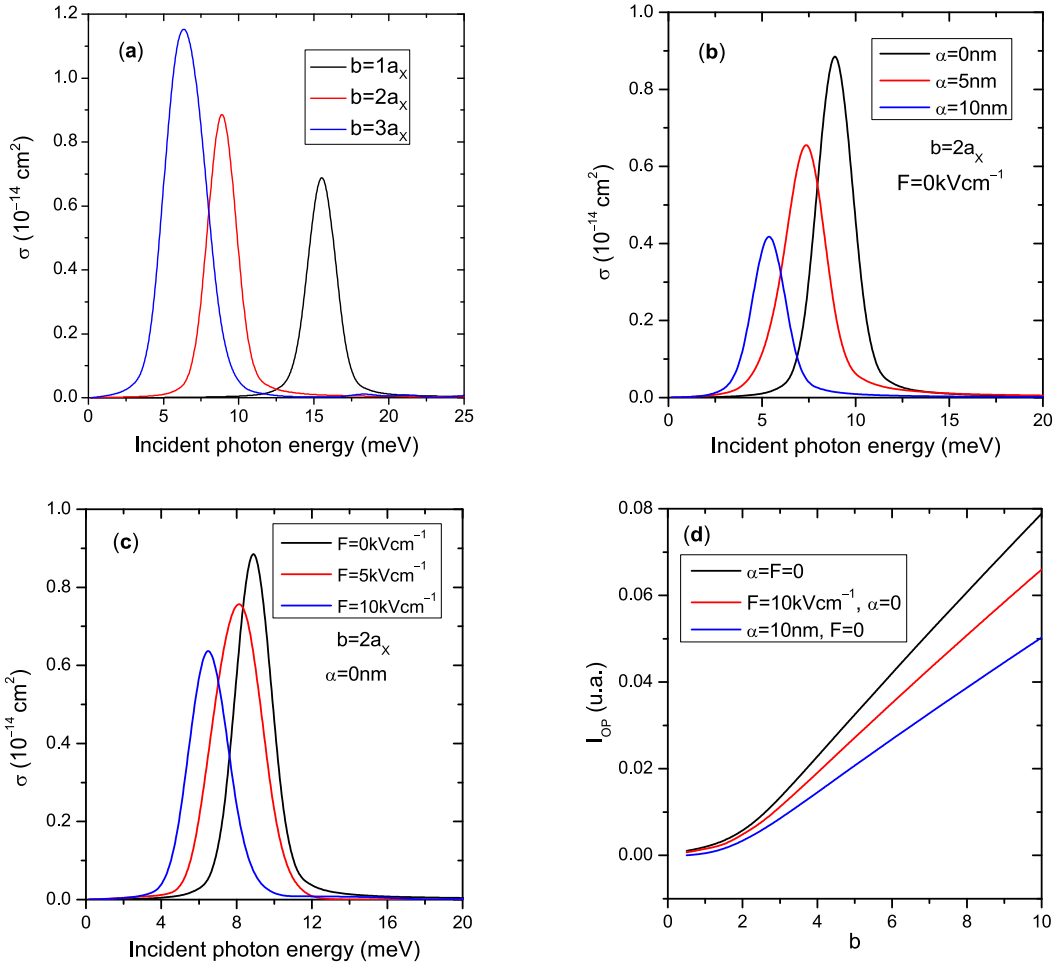

Figure 4. Photo-ionization cross-section of the exciton confined in the QD as a function of $\hbar\omega$. (**a**) For $b = 1, 2$ and $3a_X$. (**b**) For $b = 2a_X$ and for $\alpha = 0, 5$ and 10 nm). (**c**) For $b = 2a_X$ and for ($F = 0, 5$ and 10 kV/cm. (**d**) Optical integral variation versus QD radius b for $\alpha = F = 0$, α = 10 nm and $F = 10$ kV/cm.

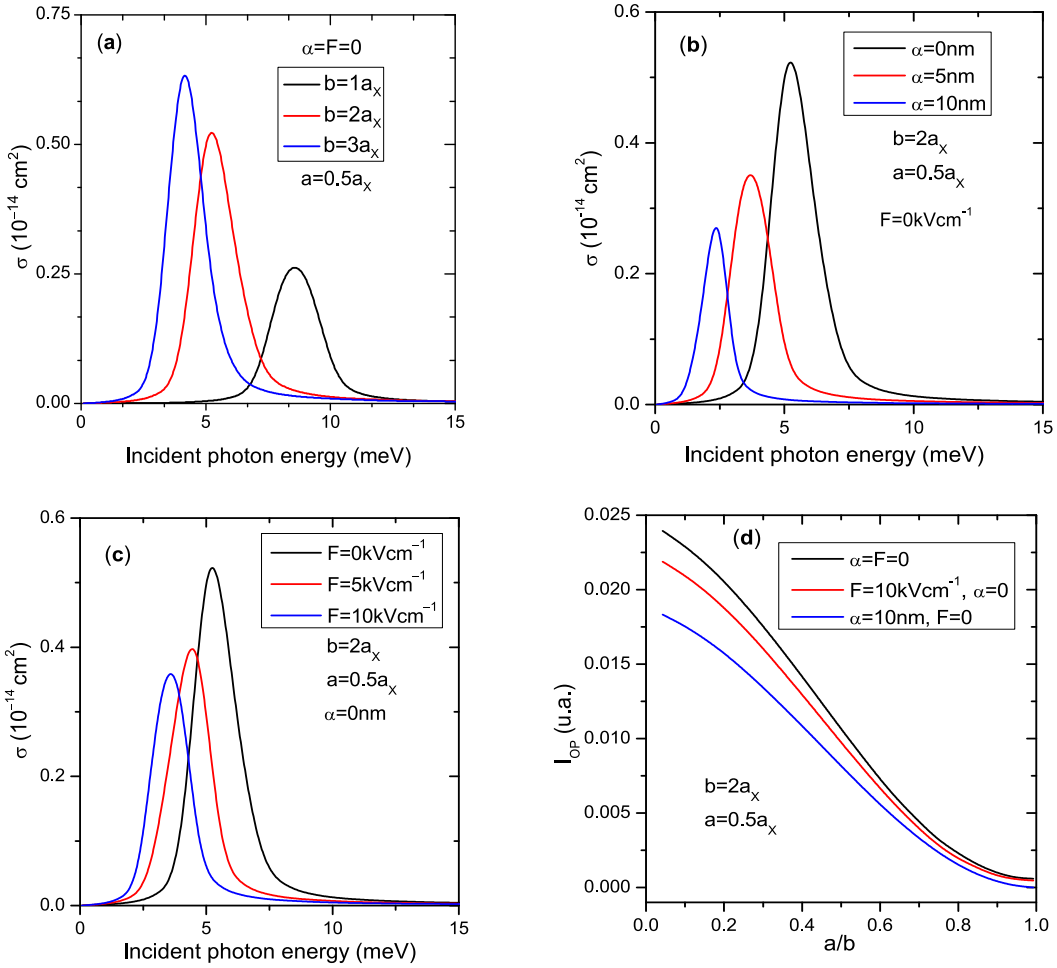

Figure 5. Photo-ionization cross-section of the exciton confined in CSQD versus $\hbar\omega$ for $a = 0.5a_X$. (**a**) For $b = 1, 2$ and $3a_X$. (**b**) For $b = 2a_X$ and for $\alpha = 0, 5$ and 10 nm). (**c**) For $b = 2a_X$ and for ($F = 0, 5$ and 10 kV/cm. (**d**) Optical integral variation versus the ratio a/b for $a = 0.5a_X$ and $b = 2a_X$ and for $\alpha = F = 0$, α = 10 nm and F =10 kV/cm.

4. Conclusions

This study investigated the influences of the ILF and EF on an exciton's electronic and optical properties confined in a spherical AlAs/GaAs/AlAs CSQD. The exciton binding energy, the mean exciton distance, and the PICS related to the exciton are computed. We have shown that the variation of sizes, laser intensity, and EF induce important changes in the localization of PICS peaks and binding energy, where the PICS peaks are red-shifted, and the excitonic E_b is decreased under these external perturbations. We have also extended our study to cover the simple quantum dot to show the core radius contribution in the exciton optical and electric properties. To our knowledge, this is the first study that has treated the effects of an ILF in the presence of an EF on the optical and electronic properties of an exciton confined in core/shell QDs. Our findings provide valuable knowledge of the behaviors of excitons within CSQD structure that can be leveraged in the development of novel coating materials with tailored optical and electronic functionalities, such as terahertz detectors by adjusting the sizes of the InAs (core) or GaAs coating (shell) materials as well as the applied external fields values.

Author Contributions: Conceptualization, N.A. and L.M.P.; methodology, N.A. and D.L.; software, N.A. and E.M.F.; formal analysis, N.A., M.E.-Y. and L.M.P.; investigation, N.A., P.D. and M.E.-Y.; resources, L.M.P., D.L.; data curation, N.A. and M.E.-Y.; writing—original draft preparation, N.A., E.M.F. and L.M.P.; writing—review and editing, N.A., L.M.P. and D.L.; visualization, L.M.P., P.D. and M.E.-Y.; supervision, D.L. and E.M.F.; project administration, L.M.P., D.L. and E.M.F. All authors have read and agreed to the published version of the manuscript.

Funding: LMP acknowledges financial support from ANID through Convocatoria Nacional Subvención a Instalación en la Academia Convocatoria Año 2021, Grant SA77210040. DL acknowledges partial financial support from Centers of Excellence with BASAL/ANID financing, AFB180001, CEDENNA. PD, LMP, and DL acknowledge partial financial support from FONDECYT 1231020.

Institutional Review Board Statement: Not applicable.

Informed Consent Statement: Not applicable.

Data Availability Statement: Not applicable.

Conflicts of Interest: The authors declare no conflict of interest.

References

1. Bimberg, D.; Grundmann, M.; Ledentsov, N.N. *Quantum Dot Heterostructures*; Wiley: New York, NY, USA, 1999.
2. Raz, T.; Ritter, D.; Bahir, G. Formation of InAs self-assembled quantum rings on InP. *Appl. Phys. Lett.* **2003**, *82*, 1706–1708. [CrossRef]
3. Zhang, D.; Lou, W.; Miao, M.; Zhang, S.C.; Chang, K. Interface-induced topological insulator transition in GaAs/Ge/GaAs quantum wells. *Phys. Rev. Lett.* **2013**, *111*, 156402. [CrossRef] [PubMed]
4. Ren, Y.; Qiao, Z.; Niu, Q. Topological phases in twodimensional materials: A review. *Rep. Prog. Phys.* **2016**, *79*, 066501. [CrossRef] [PubMed]
5. Marquardt, B.; Geller, M.; Baxevanis, B.; Pfannkuche, D.; Wieck, A.D.; Reuter, D.; Lorke, A. Transport spectroscopy of non-equilibrium many-particle spin states in self-assembled quantum dots. *Nat. Commun.* **2011**, *2*, 209. [CrossRef] [PubMed]
6. Meunier, T.; Vink, I.T.; Willems van Beveren, L.H.; Tielrooij, K.-J.; Hanson, R.; Koppens, F.H.L.; Tranitz, H.P.; Wegscheider, W.; Kouwenhoven, L.P.; Vandersypen, L.M.K. Experimental Signature of Phonon-Mediated Spin Relaxation in a Two-Electron Quantum Dot. *Phys. Rev. Lett.* **2007**, *98*, 126601. [CrossRef]
7. Fujisawa, T.; Austing, D.G.; Tokura,Y.; Hirayama, Y.; Tarucha, S. Allowed and forbidden transitions in artificial hydrogen and helium atoms. *Nature* **2002**, *419*, 278–280. [CrossRef]
8. Hofmann, A.; Maisi, V.F.; Gold, C.; Krähenmann, T.; Rössler, C.; Basset, J.; Märki, P.; Reichl, C.; Wegscheider, W.; Ensslin, K.; et al. Measuring the Degeneracy of Discrete Energy Levels Using a GaAs/AlGaAs Quantum Dot. *Phys. Rev. Lett.* **2016**, *117*, 206803. [CrossRef]
9. El Fatimy, A.; Myers-Ward, R.L.; Boyd, A.K.; Daniels, K.M.; Gaskill, D.K.; Barbara, P. Epitaxial graphene quantum dots for high-performance terahertz bolometers. *Nat. Nanotech.* **2016**, *11*, 335–338. [CrossRef]
10. Streetman, B.; Banerjee, S. *Solid State Electronic Devices*, 6th ed.; University of Texas: Austin, TX, USA, 2009.
11. Nelms, N.; Dowson, J. Goldblack coating for thermal infrared detectors. *Sens. Actuators A* **2005**, *120*, 403–407. [CrossRef]
12. Chen, Y.F.; Vela, J.; Htoon, H.; Casson, J.L.; Werder, D.J.; Bussian, D.A.; Klimov, V.I.; Hollingsworth J.A. "Giant" Multishell CdSe Nanocrystal Quantum Dots with Suppressed Blinking. *J. Am. Chem. Soc.* **2008**, *130*, 5026–5027. [CrossRef]
13. Mahler, B.; Spinicelli, P.; Buil, S.; Quelin, X.; Hermier, J.; Dubertret, B. Towards non-blinking colloidal quantum dots. *Nat. Mater.* **2008**, *7*, 659–664. [CrossRef] [PubMed]
14. Li, Z.; Yao, W.; Kong, L.; Zhao, Y.; Li, L. A General Method for the Synthesis of Ultra-Stable Core/Shell Quantum Dots by Aluminum Doping. *J. Am. Chem. Soc.* **2015**, *137*, 12430–12433. [CrossRef] [PubMed]
15. Heyes, C.D.; Kobitski, A.Y.; Breus, V.V.; Nienhaus, G.U. Effect of the shell on the blinking statistics of core-shell quantum dots: A single-particle fluorescence study. *Phys. Rev. B* **2007**, *75*, 125431. [CrossRef]
16. Vitshima, N.A.; Silwana, B.; Tsolekile, N.; Matoetoe, M.C. Effect of ZnS coating on the optoelectronic properties of aqueous glutathione capped AgInS quantum dots. *J. Alloys Compd.* **2022**, *900*, 163386. [CrossRef]
17. Yu, P.; Cao, S.; Shan, Y.; Bi, Y.; Hu, Y.; Zeng, R.; Zou, B.; Wang, Y.; Zhao, J. Highly efficient green InP-based quantum dot light-emitting diodes regulated by inner alloyed shell component. *Light Sci. Appl.* **2022**, *11*, 162. [CrossRef]
18. Bertuoli, P.T.; Baldissera, A.F.; Zattera, A.J.; Ferreira, C.A.; Alemán, C.; Armelin, E. Polyaniline coated core-shell polyacrylates: Control of film formation and coating application for corrosion protection. *Prog. Org. Coat.* **2019**, *128*, 40–51. [CrossRef]
19. Bär, M.; Lehmann, S.; Rusu, M.; Grimm, A.; Kotschau, I.; Lauermann, I.; Pistor, P.; Sokoll, S.; Schedel-Niedrig, T.; Lux-Steiner, M.C.; et al. Cd^{2+}/NH_3 treatment-induced formation of a CdSe surface layer on $CuGaSe_2$ thin-film solar cell absorbers. *Appl. Phys. Lett.* **2005**, *86*, 222107. [CrossRef]
20. Ren, Y.; Li, W.; Cao, Z.; Jiao, Y.; Xu, J.; Liu, P.; Li, S.; Li, X. Robust TiO_2 nanorods-SiO_2 core-shell coating with high-performance self-cleaning properties under visible light. *Appl. Surf. Sci.* **2020**, *509*, 145377. [CrossRef]

21. Aghoutane, N.; El-Yadri, M.; Feddi, E.; Dujardin, F.; Sadoqi, M.; Long, G. Pressure effect on an exciton in a wurtzite AlN/GaN/AlN spherical core/shell quantum dot. *MRS Commun.* **2018**, *8*, 527–532. [CrossRef]
22. Zouitine, A.; Ibral, A.; Assaid, E.; Dujardin, F.; Feddi, E. Spatial separation effect on the energies of uncorrelated and correlated electron-hole pair in CdSe/ZnS and InAs/InP core/ shell spherical quantum dots. *Superlattices Microst.* **2017**, *109*, 123–133. [CrossRef]
23. Aghoutane, N.; El-Yadri, M.; Feddi, E.; Aouami, A.; Dujardin F.; El haouari, M. Optical Absorption of Excitons in Strained Quasi 2D GaN Quantum Dot. *Phys. Status Solidi* **2019**, *256*, 1800361. [CrossRef]
24. Xie, W. Third-order nonlinear optical susceptibility and photoionization of an exciton in quantum dots. *Superlattices Microst.* **2013**, *56*, 8–15. [CrossRef]
25. Arunachalama, N.; John Peter, A.; Kyoo Yoo, C. Exciton optical absorption coefficients and refractive index changes in a strained InAs/GaAs quantum wire: The effect of the magnetic field. *J. Lumin.* **2012**, *132*, 1311–1317. [CrossRef]
26. Angayarkanni, N.; John Peter, A.; Woo Lee, C. Effects of hydrostatic pressure on intrawell and interwell excitons in a strained GaAs/GaAlAs double quantum well system. *Phys. E* **2011**, *44*, 590–596. [CrossRef]
27. Subhan, A.; Mourad, A.-H.I.; Al-Douri, Y. Influence of Laser Process Parameters, Liquid Medium, and External Field on the Synthesis of Colloidal Metal Nanoparticles Using Pulsed Laser Ablation in Liquid: A Review. *Nanomaterials* **2022**, *12*, 2144. [CrossRef] [PubMed]
28. Mostafa, A.M.; Mwafy, E.A. Synthesis of ZnO and Au@ZnO core/shell nano-catalysts by pulsed laser ablation in different liquid media. *J. Mat. Res. Technol.* **2020**, *9*, 3241–3248. [CrossRef]
29. Tsuji, T.; Iryo, K.; Watanabe, N.; Tsuji, M. Preparation of silver nanoparticles by laser ablation in solution: influence of laser wavelength on particle size. *Appl. Surf. Sci.* **2002**, *202*, 80–85. [CrossRef]
30. Hodak, J.H.; Henglein, A.; Giersig, M.; Hartland, G.V. Laser-Induced Inter-Diffusion in AuAg Core-Shell Nanoparticles. *J. Phys. Chem. B* **2000**, *104*, 11708–11718. [CrossRef]
31. Radu, A.; Kirakosyan, A.A.; Laroze, D.; Baghramyan, H.M.; Barseghyan, M.G. Electronic and intraband optical properties of single quantum rings under intense laser field radiation. *J. Appl. Phys.* **2014**, *116*, 093101. [CrossRef]
32. Ungan, F.; Bahar, M.K.; Barseghyan, M.G.; Pérez, L.M.; Laroze, D. Effect of intense laser and electric fields on nonlinear optical properties of cylindrical quantum dot with Morse potential. *Optik* **2021**, *236*, 166621. [CrossRef]
33. Barseghyan, M.G.; Mughnetsyan, V.N.; Baghramyan, H.M.; Ungan, F.; Pérez, L.M.; Laroz, D. Control of electronic and optical properties of a laser dressed double quantum dot molecule by lateral electric field. *Phys. E* **2021**, *126*, 114362. [CrossRef]
34. Tiutiunnyk, A.; Pérez-Quintana, I.; Laroze, D.; Duque, C.A.; Mora-Ramos, M.E. Influence of conduction-band non-parabolicity on terahertz intersubband Raman gain in GaAs/InGaAs step asymmetric quantum wells. *Appl. Phys. A* **2020**, *126*, 23. [CrossRef]
35. Baghramyan, H.M.; Barseghyan, M.G.; Kirakosyan, A.A.; Ojeda, J.H.; Bragard, J.; Laroze, D. Modeling of anisotropic properties of double quantum rings by the terahertz laser field. *Sci. Rep.* **2018**, *8*, 6145. [CrossRef]
36. Radu, A.; Kirakosyan, A.A.; Laroze, D.; Barseghyan, M.G. The effects of the intense laser and homogeneous electric fields on the electronic and intraband optical properties of a GaAs/$Ga_{0.7}Al_{0.3}As$ quantum ring. *Semicond. Sci. Technol.* **2015**, *30*, 045006. [CrossRef]
37. Baghramyan, H.M.; Barseghyan, M.G.; Kirakosyan, A.A.; Laroze, D. Intense Terahertz Radiation Effect on Electronic and Intraband Optical Properties of Semiconductor Quantum Rings. In *Physics of Quantum Rings*; NanoScience and Technology; Fomin, V., Ed.; Springer: Cham, Switzerland, 2018.
38. Suaza, Y.A.; Fulla, M.R.; Laroze, D.; Baghramyan, H.M.; Marin, J.H. Intense laser field effect on D_2^+ molecular complex localized in semiconductor quantum wells. *Chem. Phys. Lett.* **2019**, *730*, 384–390. [CrossRef]
39. Turkoglu, A.; Aghoutane, N.; Feddi, E.; Mora-Ramos, M.E.; Ungan, F. Non-resonant intense laser field effect on the nonlinear optical properties associated to the inter- and intra-band transitions in an anharmonic quantum well submitted to electric andmagnetic field. *Solid State Commun.* **2021**, *334*, 114390. [CrossRef]
40. Laroze, D.; Barseghyan, M.; Radu, A.; Kirakosyan, A.A. Laser driven impurity states in two-dimensional quantum dots and quantum rings. *Phys. B* **2016**, *501*, 1–4. [CrossRef]
41. Barseghyan, M.G.; Baghramyan, H.M.; Kirakosyan, A.A.; Laroze, D. The transition from double to single quantum dot induced by THz laser field. *Phys. E* **2020**, *116*, 113758. [CrossRef]
42. Ungan, F.; Mora-Ramos, M.E.; Barseghyan, M.G.; Pérez, L.M.; Laroze, D. Intersubband optical properties of a laser-dressed asymmetric triple quantum well nanostructure. *Phys. E* **2019**, *114*, 113647. [CrossRef]
43. Kasapoglu, E.; Sari, H.; Sökmen, I.; Vinasco, J.A.; Laroze, D.; Duque, C.A. Effects of intense laser field and position dependent effective mass in Razavy quantum wells and quantum dots. *Phys. E* **2021**, *126*, 114461. [CrossRef]
44. Barseghyan, M.G.; Kirakosyan, A.A.; Laroze, D. Laser driven intraband optical transitions in two-dimensional quantum dots and quantum rings. *Opt. Commun.* **2017**, *383*, 571–576. [CrossRef]
45. Yesilgul, U.; Sakiroglu, S.; Kasapoglu, E.; Sari, H.; Sökmen, I. Hydrogenic impurities in quantum dots under intense high-frequency laser field. *Phys. B* **2011**, *406*, 1441–1444. [CrossRef]
46. Lu, L.; Xie, W.; Hassanabadi, H. The effects of intense laser on nonlinear properties of shallow donor impurities in quantum dots with the Woods–Saxon potential. *J. Lumin.* **2011**, *131*, 2538–2543. [CrossRef]
47. Lu, L.; Xie, W.; Hassanabadi, H. Laser field effect on the nonlinear optical properties of donor impurities in quantum dots with Gaussian potential. *Phys. B* **2011** , *406*, 4129-04134. [CrossRef]

48. Burileanu, L.M. Photoionization cross-section of donor impurity in spherical quantum dots under electric and intense laser fields. *J. Lumin.* **2014**, *145*, 684–689. [CrossRef]
49. Wang, W.; Xu, L.; Wei, X.; Zhang, S. Intense-terahertz-laser modulated photoionization cross section of shallow-donor impurity in semiconductors in a magnetic field. *Results Phys.* **2021**, *20*, 103692. [CrossRef]
50. Isono, Y.; Morikawa, E.; Kotani, M. Two-color pulsed photoconductivity study of naphthalene single crystal: photoionization of singlet exciton. *Chem. Phys. Lett.* **1986**, *125*, 344–348. [CrossRef]
51. Feddi, E.; El Haouari, M.; Assaid, E.; Stébé, B.; El Khamkhami, J.; Dujardin, F. Magnetic field effect on the polarizability of bound polarons in quantum nanocrystallites. *Phys. Rev. B* **2003**, *68*, 235313. [CrossRef]
52. M'zerd, S.; El Haouari, M.; Aghoutane, N.; El-Yadri, M.; Feddi, E.; Dujardin, F.; Zorkani, I.; Jorio, A.; Sadoqi, M.; Long, G. Electric field effect on the photoionization cross section of a single dopant in a strained AlAs/GaAs spherical core/shell quantum dot. *J. Appl. Phys.* **2018**, *124*, 164303. [CrossRef]
53. Ouadghi, A.; Diouri, J.; Khamkhami, J. Binding energy of excitons in an infinitely deep spherical quantum dot under intense THz laser field. *Pramana J. Phys.* **2020**, *94*, 30. [CrossRef]
54. Yesilgul, U.; Ungan, F.; Kasapoglu, E.; Sari, H.; Sökmen, I. Effects of an intense, high-frequency laser field on the binding energy of excitons confined in a GaInNAs/GaAs quantum well. *Phys. B* **2012**, *407*, 528–532. [CrossRef]
55. Heyn, C.; Radu, A.; Vinasco, J.A.; Laroze, D.; Restrepo, R.L.; Tulupenko, V.; Hieu, N.N.; Phuc, H.V.; Mora-Ramos, M.E.; Ojeda, J.H.; et al. Exciton states in conical quantum dots under applied electric and magnetic fields. *Opt. Laser Technol.* **2021**, *139*, 106953. [CrossRef]
56. Niculescu, E.C.; Cristea, M.; Spandonide, A. Exciton states in CdSe/ZnS core–shell quantum dots under applied electric fields. *Superlattices Microst.* **2013**, *63*, 1–9. [CrossRef]
57. Hu, M.; Wang, H.; Gong, Q.; Wang, S. Exciton states in InGaAsP/InP core–shell quantum dots under an external electric field. *J. Comput. Electron.* **2019**, *18*, 1243–1250. [CrossRef]
58. Ehlotzky, F. Positronium decay in intense high frequency laser fields. *Phys. Lett. A* **1988**, *126*, 524–527. [CrossRef]
59. Lax, M. *Proceedings of the Atlantic City Conference on Photoconductivity*; John Wiley Sons: New York, NY, USA, 1956.
60. Barseghyan, M.G.; Hakimyfard, A.; Lopez, S.Y.; Duque, C.A.; Kirakosyan, A.A. Simultaneous effects of hydrostatic pressure and temperature on donor binding energy and photoionization cross section in pöschl–teller quantum well. *Phys. E* **2010**, *42*, 1618. [CrossRef]
61. John Peter, A. The effect of hydrostatic pressure on binding energy of impurity states in spherical quantum dots. *Phys. E* **2005**, *28*, 225–229. [CrossRef]
62. Varshni, Y.P. Effect of an intense laser field on donor impurities in spherical quantum dots. *Superlattices Microst.* **2001**, *30*, 45–52. [CrossRef]
63. Xu, T.; Yuan, L.; Fang, J. The laser-dressed potential binding energy of a hydrogenic impurity in a spherical quantum dot by the analytical transfer matrix method. *Phys. B* **2009**, *404*, 3445–3447. [CrossRef]